Journal of Materials Chemistry A

ROYAL SOCIETY OF CHEMISTRY

COMMUNICATION

View Article Online
View Journal | View Issue

Cite this: J. Mater. Chem. A, 2022, 10, 19635

Received 21st March 2022
Accepted 23rd May 2022

DOI: 10.1039/d2ta02259a

rsc.li/materials-a

Effects of Stokes shift and Purcell enhancement on fluorescence-assisted radiative cooling†

Xue Ma,[a] Yang Fu,[a] Arsenii Portniagin,[a] Ning Yang,[b] Danjun Liu,[a] Andrey L. Rogach,[a] Jian-Guo Dai[b] and Dangyuan Lei *[a]

Passive daytime radiative cooling has been widely investigated ascribed to the great potential in combatting energy crisis and global warming. Polymeric coatings comprising functional fillers with solar reflectance and infrared emissivity both over 0.9 have proven to be particularly effective for sub-ambient daytime radiative cooling. However, the intrinsic absorption of many functional fillers with optical bandgaps within the solar spectrum reduces the cooling potential and consequently limits material choices. It has recently been demonstrated that introducing fluorescent materials into polymeric coatings can convert the absorbed sunlight to fluorescent emissions and hence increase the effective solar reflectance and cooling performance. In this work, we carry out a systematic experimental investigation on the influence of Stokes shift and Purcell enhancement in such fluorescence-mediated radiative cooling. We find that using phosphors with smaller Stokes shifts and nanoparticle fillers of appropriate sizes can significantly enhance the effective solar reflectance. We show that matching the emission wavelengths of two phosphors with the Mie scattering resonance wavelengths of the TiO_2 nanoparticle fillers shortens their fluorescence lifetimes by 61% and 23%, respectively, indicating Purcell enhancement factors of 2.6 and 1.3 and ultimately increasing the effective solar reflectance of the fluorescent coatings by up to ~4% in field tests. The fluorescence enhancement approach demonstrated here provides an effective strategy for making radiative cooling coatings compatible with commercially available inexpensive engineering materials and potential for realizing colored coatings.

Introduction

The excessive energy consumption for refrigeration in buildings aggravates the global energy crisis and the greenhouse effect.[1,2] Recently, passive daytime radiative cooling has emerged as a promising alternative to conventional air conditioning since this technology does not consume any electricity.[3–5] A radiative cooling material can emit thermal radiation to the extremely

[a]Department of Materials Science and Engineering, The Hong Kong Institute of Clean Energy, Centre for Functional Photonics (CFP), City University of Hong Kong, 83 Tat Chee Avenue, Kowloon, Hong Kong, 999077, China. E-mail: dangylei@cityu.edu.hk
[b]Department of Civil and Environmental Engineering, The Hong Kong Polytechnic University, Hung Hom, Kowloon, Hong Kong, 999077, China

† Electronic supplementary information (ESI) available. See https://doi.org/10.1039/d2ta02259a

Dangyuan Lei is an Associate Professor at the Department of Materials Science and Engineering in the City University of Hong Kong. He received his BSc, MPhil and PhD degrees all in Physics from Northwest University, The Chinese University of Hong Kong and Imperial College London in 2005, 2007 and 2011, respectively. His research interest centers on nanophotonics and low-dimensional quantum materials, with particular interest in cavity-enhanced light–matter interaction at the nanoscale and applications in miniaturized photonic and optoelectronic devices, sensing, imaging, energy harvesting, conversion and saving. He has co-authored 182 publications, received 7900 citations and an h-index of 52 (Google Scholar as of May 2022), and given 4 keynote speeches and >80 invited talks.

cold outer space at a temperature of 3 K (−270 °C) through the atmospheric transparent window (8–13 μm).[6–8] To achieve sub-ambient daytime cooling even under direct sunlight irradiation, radiative cooling materials require both high reflectance in the highly intensive solar spectrum (0.3–2.5 μm) and high emissivity in the mid- and even far-infrared regions. After the first demonstration of sub-ambient daytime radiative cooling in 2014,[9] versatile radiative cooling systems have been designed and investigated, mainly including photonic structures,[10–12] metamaterials,[13–17] porous structures[18–21] and polymer coatings.[22–26]

Among the abovementioned systems, polymeric coatings based on matrix–filler composites exhibit multiple superiorities, such as cost effectiveness, ease in production and good durability, making them a promising candidate for scalable applications. A polymer cooling coating often consists of a polymer matrix that provides primary infrared radiation and functional fillers to enhance solar reflection or to further improve infrared emission. For the former purpose, various polymers (polymethyl methacrylate, polydimethylsiloxane, polymethylpentene, poly(vinylidene fluoride-*co*-hexafluoropropene) *etc.*) have been employed owing to the rich vibrational modes of their functional groups, which lead to fingerprint infrared absorption bands within the atmospheric transparency window. According to Kirchhoff's thermal law, such vibration absorption enables a plenty of infrared radiation. Moreover, the transparent appearance of the polymer matrix due to the low extinction coefficient within the solar spectral region is also preferred to diminish solar absorption. For the latter purpose, semiconductors with large optical bandgap and high indices of refraction are favorable functional fillers with pronounced Mie scattering that enhances the overall solar reflectance. Among the reported fillers, $BaSO_4$ nanoparticles have proven to be a good candidate for making ultra-white radiative cooling coatings due to a large bandgap of ~6 eV.[23] However, the refractive index of $BaSO_4$ is not sufficiently high (~1.6) compared to that of most polymer matrices (1.4–1.5), which limits the efficiency of sunlight multiple scattering and hence requires a high volume density for efficient cooling. TiO_2 nanoparticles (NPs), as a common component in commercial white coatings, manifest a high refractive index of ~2.5 and extraordinary visible-light reflectance.[27] However, TiO_2 has severe UV absorption that restricts the solar reflectance of TiO_2-based coatings to be typically below 90%. To overcome this issue, a fluorescence-assisted strategy has recently been proposed and demonstrated for improving the solar reflectance of TiO_2-based polymeric coatings.[24,28–31] By introducing fluorescent pigments into a TiO_2-based white coating, the UV light absorbed can be converted and re-emitted as visible light. However, the relationship between the optical properties of fluorescent materials and the corresponding solar reflectance enhancement remains elusive, which needs to be further investigated.

In this work, we experimentally demonstrate a significant Purcell enhancement in a fluorescent polymer coating in which matching the emission spectrum of fluorescent pigments with the Mie scattering resonance modes of TiO_2 NPs leads to the lifetime reduction up to 61% and a Purcell factor of 2.6. By comparing the impact of two different commercial phosphors ($BaMgAl_{10}O_{17}:Eu^{2+}$ and (Sr, Ba)$SiO_4:Eu^{2+}$) on the cooling performance of the resultant coatings, we reveal that the phosphor with a smaller Stokes shift is preferred to enhance the effective solar reflectance. Our field tests show an increase of up to ~4% in the effective solar reflectance. Our study provides important insights into fluorescence-assisted radiative cooling and ultimately broadens the materials selection for commercialization of the contemporary daytime radiative cooling coating technology.

Results and discussion

It has been demonstrated that the photoluminescence (PL) lifetime of fluorescent pigments can be reduced after being added into TiO_2-based coatings, indicating a Purcell effect in the coating system.[24] When large amounts of TiO_2 NPs are located at the vicinity of fluorescence pigments, the shell assembled by TiO_2 NPs is in analogy to an optical cavity which can enhance the spontaneous radiation of the fluorescent material (Fig. 1a). To investigate the impact of phosphors on the cooling performance, a series of TiO_2-based coatings were prepared and compared. An eco-friendly waterborne emulsion, poly-styrene-acrylic, with good durability and sustainability was

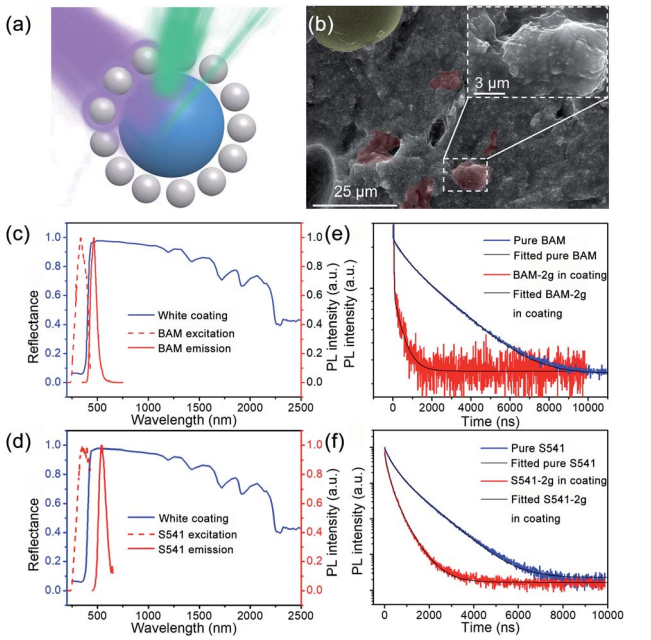

Fig. 1 (a) Schematic of Purcell enhancement for a fluorescent microparticle attached with TiO_2 NPs. (b) SEM image of a fluorescent cooling coating consisting of hollow glass spheres (yellow region), fluorescent pigments (red regions) and TiO_2 NPs (white dots). The inset shows enlarged view of a fluorescent microparticle. (c and d) Solar reflectance of a TiO_2 NP-based white coating and the excitation and emission spectra of (c) BAM and (d) S541. (e) Measured PL decay curves for pure BAM (blue) and BAM in the white coating (red), and the corresponding fitting results (black). (f) Measured PL decay curves for pure S541 (blue) and S541 in the white coating (red), and the corresponding fitting results (black).

employed as the polymer matrix to provide primary infrared emission.[24] Hollow glass microspheres were also added to improve infrared emissivity benefited from the surface phonon-polariton resonance supported at ~9 μm. During the production of the polymer cooling coating, functional fillers were always randomly dispersed within the polymer matrix. Micro-sized phosphors would be surrounded by plenty of TiO_2 nanoparticles adjacent to the surface, as shown in Fig. 1b. Two phosphors, $BaMgAl_{10}O_{17}:Eu^{2+}$ (BAM) and (Sr, Ba)$SiO_4:Eu^{2+}$ (S541), with different PL spectra were chosen to study the impact of their optical properties on the cooling effect. Due to the energy loss during photon conversion of down-conversion materials, it is obvious that high quantum efficiency is favorable for phosphors to diminish solar absorption of the fluorescent cooling coating. The quantum yields of BAM and S541 are both ~ 90%, which are higher than those of $SrAl_2O_4:Eu^{2+}$, Dy^{3+}, and Yb^{3+} used in the previous study (see Table S5†).[24] Fig. 1c and d demonstrate the excitation and emission spectra of BAM and S541, in comparison with the reflectance spectra of TiO_2-based white coatings without phosphors. The overall solar reflectance is 0.88 which is contributed mainly from TiO_2 NPs (see Fig. S6†). The excitation peaks of BAM (~333 nm) and S541 (~341 nm) are located within the UV absorption region of TiO_2, which means that phosphors can compete with TiO_2 in the absorption of UV light. The emission peak of BAM (463 nm) has shorter wavelength than that of S541 (539 nm). The spectral profiles of emission peaks of two phosphors are very similar, while S541 has larger Stokes shift than BAM. Further, the PL lifetime of both phosphors were characterized. As illustrated in Fig. 1e and f, both phosphors exhibit an obvious decrease in the PL lifetime after being added into the cooling coating. The biexponential fitting of lifetime decay curves was performed by using the following equation:

$$I(t) = I_0 + A_1 \exp\left(-\frac{t}{\tau_1}\right) + A_2 \exp\left(-\frac{t}{\tau_2}\right), \quad (1)$$

where τ_1 and τ_2 are non-radiative and radiative lifetimes, respectively. A_1 and A_2 are amplitudes for non-radiative and radiative decay, respectively. The fitting results in Table S1† show that the radiative lifetime τ_2 was shortened by about 61% for BAM and 23% for S541, which means that phosphors' spontaneous emission rate is enhanced by their environment, mimicking the Purcell effect in optical cavities. The Purcell factor can be calculated through the fitted radiative lifetime as:[32]

$$F_P = \frac{1/\tau_{2,coat}}{1/\tau_{2,pure}}, \quad (2)$$

where $\tau_{2,coat}$ and $\tau_{2,pure}$ represent the radiative lifetimes of phosphors in the cooling coating and of pure phosphor, respectively. Therefore, Purcell factors of 2.6 for BAM and 1.3 for S541 can be achieved. As the lifetimes were shortened, more photons converted by phosphors will be emitted in the unit time, which increases the PL power intensity and boosts solar reflectance for fluorescent cooling coatings.

According to Mie scattering theory, light will be scattered by TiO_2 NPs with optical sizes that are comparable to the wavelength.[33,34] The scattering cross section is much larger than the physical cross section of TiO_2 NPs and distorts the adjacent local field.[35] Due to the presence of the adjacent TiO_2 NPs, the surrounding dielectric environment of fluorescent microparticles is significantly modulated. Moreover, multiple scattering occurs among the TiO_2 NPs and elongates the existing time of light. Two requirements for increasing the emission rate, confining light spatially and temporally, are thus satisfied, which enable the Purcell enhancement.[32,36–38] To obtain higher Purcell enhancement, scattering features of TiO_2 NPs should be matched with the emission spectra of phosphors. For ideally spherical TiO_2 NPs with a uniform diameter, as considered in most previous studies, it is convenient to calculate the scattering cross section or the scattering efficiency based on Mie theory. However, commercial TiO_2 powder consists of TiO_2 NPs with non-uniform sizes and irregular morphology, indicating non-analytical scattering. Thus, we implemented *in situ* dark-field scattering (DFS) measurement to investigate the scattering features of commercial TiO_2 powder. For single particle characterization, the TiO_2–water suspension was sprayed onto a glass substrate to sparsely disperse TiO_2 NPs. The optical image under a dark-field microscope and the corresponding scanning electron microscopy (SEM) image are shown in Fig. 2a and b, respectively. Yellow-green appearance can be observed for most single TiO_2 NPs while white for TiO_2 clusters as shown in Fig. 1a. Six single TiO_2 NPs were selected for DFS measurement and *in situ* SEM imaging. As shown in Fig. 2c–h, all the TiO_2 NPs manifest non-ideal geometries, which can be regarded as quasi-sphere, rod, triangular, *etc.* The scattering peaks of TiO_2 NPs mainly distribute within 450–600 nm, which are

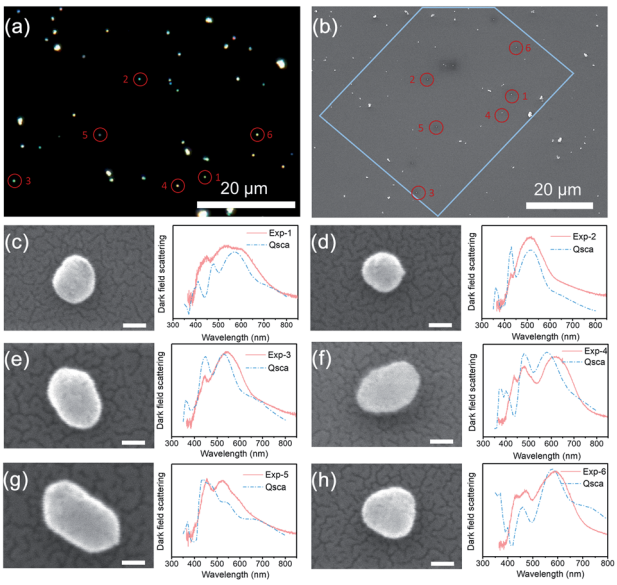

Fig. 2 (a) Optical DFS image of TiO_2 NPs on the glass substrate. (b) *In situ* SEM image of the TiO_2 NPs in (a). (c–h) Left panel: zoom-in SEM image for single TiO_2 NPs numbered 1–6 in (a and b); right panel: corresponding experimental DFS spectra (pink solid lines) and simulated scattering efficiency Q_{sca} (blue dashed lines). The scale bar is 100 nm in (c–h).

exactly the wavelength range of yellow-green light. More peaks emerge for TiO_2 NPs with higher irregularity. Further numerical simulations for DFS spectra of TiO_2 NPs were carried out with extracted geometry from the SEM image. Good agreement in scattering peaks was obtained and is shown in Fig. 2d, e and g, in which the morphologies were well reconfigured. For TiO_2 NPs that are hard to reconfigure in simulations, only the spectral envelope could be reproduced as shown in Fig. 2c, f and h. The high scattering efficiency after 450 nm provides moderate dielectric regulation, leading to modulation of spontaneous emission of both BAM and S541. It should be noted that only TiO_2 NPs with suitable sizes can be recognized in the DFS measurement due to low accuracy for small particles (<50 nm) and difficulties in distinguishing large particles (>400 nm) from clusters. Therefore, we chose TiO_2 powder with particle sizes centred at ~200 nm. When added into the polymer matrix, higher refractive index of the polymer than air will slightly change the scattering peak into a shorter wavelength one (see Fig. S2†). Therefore, the emission peak of BAM better matches TiO_2 scattering in the coating than that of S541, which contributes to the higher Purcell factor of BAM. For TiO_2 powders with smaller or larger size distributions (see Fig. S3†), peak scattering deviates from the emission spectra of phosphors, resulting in ignorable dielectric modulation and thus the Purcell enhancement. Nearly no lifetime reduction can be observed for other TiO_2 powders (see Fig. S7†).

After the preparation of fluorescent cooling coatings based on BAM and S541, field tests were executed to evaluate the cooling performance. A white coating without phosphor was also prepared for comparison. All the coatings were sprayed on cement boards and placed on top of thermally insulated boxes. To compare the effect of two phosphors, we added the same amounts of phosphors into the white coating. As shown in Fig. 3a and b, all cooling coatings with or without phosphor can achieve obvious sub-ambient cooling during the daytime under typical winter clear sky in Hong Kong. As the solar intensity increases at noontime, smaller temperature reduction was obtained ascribing to solar absorption of TiO_2 NPs. The coating added with BAM showed lower temperature than others, and the cooling effect of the S541-based coating was very similar to that of the white coating without phosphors. This is because S541 has larger Stokes shift and less Purcell enhancement than BAM, which means more energy from UV light has been converted into heat. To further optimize the amounts of phosphors, we made two series of cooling coatings with different contents of phosphors. It has been illustrated in Fig. 3c that the temperatures of cooling coatings are ~15 °C lower than that of the uncoated cement board. From the enlarged temperature changing curve shown in Fig. 3d, the coating with 2 g BAM shows the best cooling performance, while the one with 2 g S541 shows no sub-ambient cooling before 14:00. Other coatings with higher amounts of phosphors show a temperature above ambient temperature during the noontime (10:00–14:00) since the excessive use of phosphors may introduce extra solar absorption through non-radiative recombination.

To quantify the impact of phosphors, effective solar reflectance (ESR) should be evaluated. Since the commercial UV/vis/

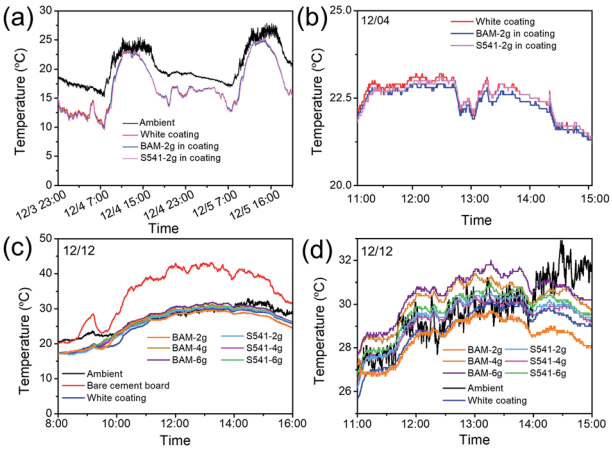

Fig. 3 (a) Recorded temperature curves of the ambient (black), white coating without phosphors (red) and two fluorescent cooling coatings (blue and pink) in sunny winter days in Hong Kong. (b) Enlarged view of (a) on December 4. (c) Field test results for the ambient, white coating, bare cement board, and fluorescent cooling coatings with different phosphors and varying concentrations on December 12. (d) Enlarged view of (c) during the noon time.

NIR spectrometer cannot measure the absolute spectral reflectance of fluorescent materials, a calorimetric method was adopted here for analysing the ESR of our fluorescent cooling coatings. Based on standard linearization of long-wave radiative exchange and approximation on the radiative heat transfer coefficient, the surface temperature of the fluorescent cooling coating can be expressed as:[39]

$$T \cong \frac{[(1-\mathrm{ESR})I_{\mathrm{solar}} + h_{\mathrm{non\text{-}rad}}T_{\mathrm{amb}} + h_{\mathrm{rad}}T_{\mathrm{atm}}]}{h_{\mathrm{non\text{-}rad}} + h_{\mathrm{rad}}}, \quad (3)$$

where I_{solar} is the solar intensity; h_{rad} and $h_{\mathrm{non\text{-}rad}}$ are radiative and non-radiative heat transfer coefficients, respectively; T_{amb}

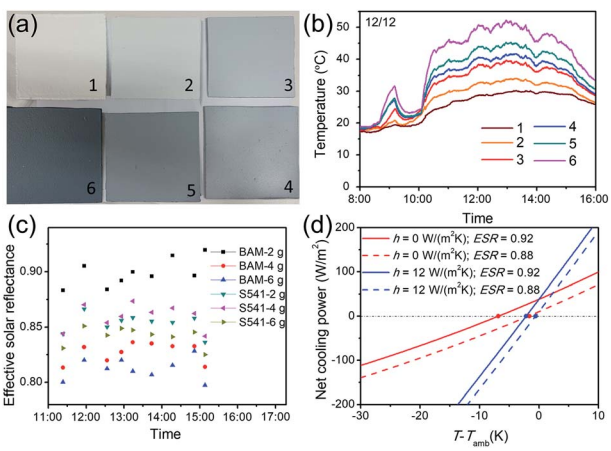

Fig. 4 (a) Optical images of six reference coatings without phosphors. (b) Field test results of the six reference coatings on December 12. (c) Fitted ESR for six fluorescent cooling coatings at noon time. (d) Calculated net cooling power for coatings with different ESR values and non-radiative heat transfer coefficients h. The solar intensity, downward longwave radiation and coating emissivity for modelling were kept as 700 W m^{-2}, 360 W m^{-2} and 0.95, respectively.

and T_{atm} are the temperature of ambient air and atmosphere, respectively. This equation can be further determined by fitting a linear line of the form:

$$T = a \times \mathrm{ESR} + b, \quad (4)$$

where a and b are simplified environmental parameters. Therefore, ESR of fluorescent cooling coatings can be obtained from eqn (4) with adequate reference samples. In view of this, we made 6 reference samples based on the white cooling coating, in which different concentrations of the black pigment and no phosphors were added, as shown in Fig. 4a. All reference samples were also sprayed on cement boards. The reflectance decreases with the increase of the pigment amount (Fig. S9 and Table S3†). To verify the relationship between their surface temperature and solar reflectance, all samples were placed under direct sunlight and the temperature was measured by using thermocouples. As shown in Fig. 4b, the samples with lower reflectance had higher temperature after being exposed to sunlight. The temperature data were then fitted using eqn (4). The temperature of reference coatings varies nearly linearly with the total solar reflectance (see Fig. S11†). The simplified environmental parameters a and b can be extracted. Thus, the ESR of fluorescence coatings can be obtained through the fitting results and temperature shown in Fig. 3c. Fig. 4c provides fitted ESR for six fluorescent cooling coatings at noon time. ESR for cooling coatings with S541 phosphors and cooling coatings with high concentration of BAM phosphors is all lower than 0.88, indicating no superiority to the white coating. Only the coating with 2 g BAM exhibits the average ESR higher than 0.88 due to the moderate Stokes shift and high Purcell factor. An ESR improvement of up to ~0.04 can be achieved, which provides a promising approach for upgrading commercial cooling coatings. As shown in Fig. 4d, though the temperature reduction was not obvious due to large non-radiative heat transfer coefficient h, the ESR improvement can facilitate 28 W m^{-2} cooling power improvement. Compared to previous fluorescent cooling coatings, the BAM-based coating delivers higher ESR improvement ascribing to stronger Purcell enhancement and higher quantum yield, while the superiority was slightly restricted by the large Stokes shift (see Table S5†), which can be further improved through materials optimization.

Experimental

Sample preparation

The preparation of the fluorescence cooling coating was performed as follows: 20 g poly-styrene-acrylic emulsion (EC-702, BASF (China) Co. Ltd.), 12 g TiO_2 nanoparticles (Ti-Pure® R902, DuPont™), phosphor (Shenzhen Looking Long Technology Co. Ltd.) and an appropriate amount of water were first mixed in a 50 mL beaker under continuous stirring, followed by the addition of 0.4 g dispersant agent (polycarboxylate sodium salt), 0.2 g suspension agent (associative polyurethane) and 0.24 g leveling agent (polyurethane). The mixture was stirred at 800 rpm min^{-1} for one hour. Then the stirring speed was reduced to 400 rpm min^{-1} and 3 g hollow glass microspheres (Glass Bubble K25, 3M™), 0.4 g anti foaming agent (mineral oil) and 1 g film-forming agent (Texanol) were added. All the agents were purchased from Guangzhou Run Hong Chemical Co. Ltd. After 30 min of stirring, the mixture was sprayed evenly on the cement board using a spray gun under a pressure of 5 MPa.

In situ dark-field scattering measurements

The dark-field scattering spectra of TiO_2 nanoparticles were measured on a customized upright microscope system (Olympus, BX51). The sample was illuminated with a white light source after being focused with a 100× dark-field objective (NA = 0.8). The cross-section of the coating and single TiO_2 nanoparticles was characterized by using an FEI Quanta 450 field-emission scanning electron microscope at a voltage of 15 kV.

Optical properties of coatings and size distribution characterization

Reflectance spectra of white coating and reference samples were measured on a PerkinElmer Lambda 1050+ UV/vis/NIR wide band spectrometer equipped with an integrating sphere. Excitation spectra, emission spectra, PL lifetime and quantum yield of pure phosphors/fluorescent cooling coatings were collected on an Edinburgh Instruments FLS900 fluorescence spectrometer. The size distributions of TiO_2 powders and fluorescent pigments were characterized by using a Malvern Mastersizer 3000 particle size analyser.

Field test

The apparatus for the field test is shown in Fig. S8a.† The samples consisting of coatings sprayed on commercially available cement boards were placed on an Al-foil-covered foam box without the polyethylene cover. K-Type thermocouples were embedded into the cement boards near the coated surfaces for measuring the sample temperature. One thermocouple was placed in a louver box to measure the ambient temperature. The real-time temperatures of coatings and ambient air were recorded on a multichannel data logger (MEMORY HiLOGGER LR8431-30, Hioki E.E. Co.). Solar intensity and relative humidity were recorded by using a pyranometer (MS-802, EKO Instruments) and a mini weather station (WS601-UMB, Lufft).

Conclusions

In this work, we demonstrate that fluorescent pigments provide further improvement for the performance of radiative cooling coatings based on commercial TiO_2 powders. Our investigations show that various parameters can affect the contribution of phosphors to the cooling performance. Through matching the emission spectra of the phosphors with the scattering resonance modes of the adjacent TiO_2 NPs, the surrounding electromagnetic environment is modified, and the spontaneous emission rate of phosphors is accelerated through the Purcell enhancement mechanism. Further field tests demonstrated that BAM with smaller Stokes shift and higher Purcell factor is preferred to S541 to diminish energy loss during photon conversion. An improvement in solar reflectance of up to ~4%

was achieved by adding adequate BAM into the TiO_2-based white coating, which can be further improved by minimizing the Stokes shift. Our work has provided further understanding on fluorescence-assisted radiative cooling and paved the way for commercialization of fluorescent cooling coatings.

Author contributions

Xue Ma and Yang Fu contributed equally to this work. Xue Ma: conceptualization, investigation, and writing. Yang Fu: investigation, methodology and writing. Arsenii Portniagin and Andrey L. Rogach: investigation. Ning Yang: investigation. Danjun Liu: investigation. Jian-Guo Dai: supervision. Dangyuan Lei: conceptualization and supervision.

Conflicts of interest

There are no conflicts to declare.

Acknowledgements

We acknowledge the financial support by the City University of Hong Kong (APRC Project No. 9610434, and Centre for Functional Photonics) and the Research Grants Council of Hong Kong (GRF Project No. 15223120).

Notes and references

1 B. I. Cook, J. E. Smerdon, R. Seager and S. Coats, *Clim. Dyn.*, 2014, **43**, 2607–2627.
2 J. Henley, *The Guardian*, 2015, vol. 26.
3 D. Zhao, A. Aili, Y. Zhai, S. Xu, G. Tan, X. Yin and R. Yang, *Appl. Phys. Rev.*, 2019, **6**, 021306.
4 J. Mandal, Y. Yang, N. Yu and A. P. Raman, *Joule*, 2020, **4**, 1350–1356.
5 J. A. Reagan and D. Acklam, *Energy Build.*, 1979, **2**, 237–248.
6 C. Granqvist and A. Hjortsberg, *J. Appl. Phys.*, 1981, **52**, 4205–4220.
7 S. Fan and W. Li, *Nat. Photonics*, 2022, 1–9.
8 X. Yin, R. Yang, G. Tan and S. Fan, *Science*, 2020, **370**, 786–791.
9 A. P. Raman, M. A. Anoma, L. Zhu, E. Rephaeli and S. Fan, *Nature*, 2014, **515**, 540–544.
10 D. Chae, M. Kim, P.-H. Jung, S. Son, J. Seo, Y. Liu, B. J. Lee and H. Lee, *ACS Appl. Mater. Interfaces*, 2020, **12**, 8073–8081.
11 H. Ma, K. Yao, S. Dou, M. Xiao, M. Dai, L. Wang, H. Zhao, J. Zhao, Y. Li and Y. Zhan, *Sol. Energy Mater. Sol. Cells*, 2020, **212**, 110584.
12 Y. Fu, J. Yang, Y. Su, W. Du and Y. Ma, *Sol. Energy Mater. Sol. Cells*, 2019, **191**, 50–54.
13 Y. Zhai, Y. Ma, S. N. David, D. Zhao, R. Lou, G. Tan, R. Yang and X. Yin, *Science*, 2017, **355**, 1062–1066.
14 C. Zou, G. Ren, M. M. Hossain, S. Nirantar, W. Withayachumnankul, T. Ahmed, M. Bhaskaran, S. Sriram, M. Gu and C. Fumeaux, *Adv. Opt. Mater.*, 2017, **5**, 1700460.
15 S. Jeong, C. Y. Tso, Y. M. Wong, C. Y. Chao and B. Huang, *Sol. Energy Mater. Sol. Cells*, 2020, **206**, 110296.
16 H. Zhang, K. C. Ly, X. Liu, Z. Chen, M. Yan, Z. Wu, X. Wang, Y. Zheng, H. Zhou and T. Fan, *Proc. Natl. Acad. Sci. U. S. A.*, 2020, **117**, 14657–14666.
17 S.-Y. Heo, G. J. Lee, D. H. Kim, Y. J. Kim, S. Ishii, M. S. Kim, T. J. Seok, B. J. Lee, H. Lee and Y. M. Song, *Sci. Adv.*, 2020, **6**, eabb1906.
18 J. Mandal, Y. Fu, A. C. Overvig, M. Jia, K. Sun, N. N. Shi, H. Zhou, X. Xiao, N. Yu and Y. Yang, *Science*, 2018, **362**, 315–319.
19 T. Wang, Y. Wu, L. Shi, X. Hu, M. Chen and L. Wu, *Nat. Commun.*, 2021, **12**, 1–11.
20 D. Li, X. Liu, W. Li, Z. Lin, B. Zhu, Z. Li, J. Li, B. Li, S. Fan and J. Xie, *Nat. Nanotechnol.*, 2021, **16**, 153–158.
21 A. Leroy, B. Bhatia, C. C. Kelsall, A. Castillejo-Cuberos, M. Di Capua H, L. Zhao, L. Zhang, A. Guzman and E. Wang, *Sci. Adv.*, 2019, **5**, eaat9480.
22 X. Li, J. Peoples, Z. Huang, Z. Zhao, J. Qiu and X. Ruan, *Cell Rep. Phys. Sci.*, 2020, **1**, 100221.
23 X. Li, J. Peoples, P. Yao and X. Ruan, *ACS Appl. Mater. Interfaces*, 2021, **13**, 21733–21739.
24 X. Xue, M. Qiu, Y. Li, Q. Zhang, S. Li, Z. Yang, C. Feng, W. Zhang, J. G. Dai and D. Lei, *Adv. Mater.*, 2020, **32**, 1906751.
25 Y. Liu, A. Bai, Z. Fang, Y. Ni, C. Lu and Z. Xu, *Materials*, 2019, **12**, 1208.
26 Y. Chen, B. Dang, J. Fu, C. Wang, C. Li, Q. Sun and H. Li, *Nano Lett.*, 2020, **21**, 397–404.
27 Y. Fu, Y. An, Y. Xu, J. G. Dai and D. Lei, *EcoMat*, 2022, **4**, e12169.
28 S. Son, S. Jeon, D. Chae, S. Y. Lee, Y. Liu, H. Lim, S. J. Oh and H. Lee, *Nano Energy*, 2021, **79**, 105461.
29 S. Jeon, S. Son, S. Y. Lee, D. Chae, J. H. Bae, H. Lee and S. J. Oh, *ACS Appl. Mater. Interfaces*, 2020, **12**, 54763–54772.
30 R. A. Yalçın, E. Blandre, K. Joulain and J. Drévillon, *J. Photonics Energy*, 2021, **11**, 032104.
31 P. Berdahl, S. S. Chen, H. Destaillats, T. W. Kirchstetter, R. M. Levinson and M. A. Zalich, *Sol. Energy Mater. Sol. Cells*, 2016, **157**, 312–317.
32 B. Romeira and A. Fiore, *IEEE J. Quantum Electron.*, 2018, **54**, 1–12.
33 Z. Huang and X. Ruan, *Int. J. Heat Mass Transfer*, 2017, **104**, 890–896.
34 J. Peoples, X. Li, Y. Lv, J. Qiu, Z. Huang and X. Ruan, *Int. J. Heat Mass Transfer*, 2019, **131**, 487–494.
35 Y. Tanaka, G. Obara, A. Zenidaka, N. N. Nedyalkov, M. Terakawa and M. Obara, *Opt. Express*, 2010, **18**, 27226–27237.
36 E. M. Purcell, in *Confined Electrons and Photons*, Springer, 1995, pp. 839–839.
37 D. Englund, A. Faraon, I. Fushman, N. Stoltz, P. Petroff and J. Vučković, *Nature*, 2007, **450**, 857–861.
38 Y. Yamamoto, S. Machida and G. Björk, *Phys. Rev. A: At., Mol., Opt. Phys.*, 1991, **44**, 657.
39 R. Levinson, S. Chen, C. Ferrari, P. Berdahl and J. Slack, *Energy Build.*, 2017, **152**, 752–765.

